Hybrid Hamiltonian Spectral Analysis: Exploring the Rodeo Algorithm

Tom Dodd

Abstract

We examine the properties of the rodeo algorithm of Choi et al. in detail. In particular, we clarify and expand on the arguments of the original two papers, particularly regarding the claimed asymptotic behaviours and time complexity for preparing a particular energy eigenstate. Using the example of a simple one-qubit Hamiltonian, we also support an assumption made about the distribution used for the generation of random evolution times and show explicit examples of the exponential suppression of orthogonal energy eigenstates. Finally, we use a simulation of IBM Q hardware to attempt to estimate the energy eigenvalues and prepare the ground state of a randomly generated two-qubit Hamiltonian.

1 Introduction

Across the entire field of quantum computing, it is often the case that a quantum algorithm requires a very particular quantum state for further processing, such as when analysing the ground states of particular molecular or condensed matter systems [6]. It is also important in some branches of quantum machine learning [7].

Such an algorithm would require the use of a quantum state preparation subroutine, which can be achieved with multiple uses of the phase estimation algorithm as part of a larger process which also makes use of classical statistics [8] [19].

The rodeo algorithm [4] is a simple modification of the original phase estimation circuit, which substitutes quantum circuit complexity for additional quantum circuit executions and classical processing between iterations. The use of this algorithm for the eigenvalue estimation of a one-qubit Hamiltonian has been demonstrated, on the IBM Q Casablanca device, to surpass the accuracy of attempting to directly prepare the eigenstates and measure their corresponding eigenvalues [11]. Throughout, we will use units in which $\hbar = 1$.

2 Quantum Phase Estimation

Quantum phase estimation (QPE), the initial ideas for which were introduced in 1995 by Alexei Kitaev [8], is a critical subroutine in some of the most important quantum computing algorithms that provide a theoretical speedup over their classical counterparts, most famously Shor's algorithm for prime factorisation [15] and the HHL algorithm for analysing linear systems [5]. Its primary purpose is to estimate the phase of the eigenvalue of a unitary operator $\hat{U}$ corresponding to one of its pre-prepared eigenstates $|\psi\rangle$ [9]. The circuit diagram is shown in figure 1.

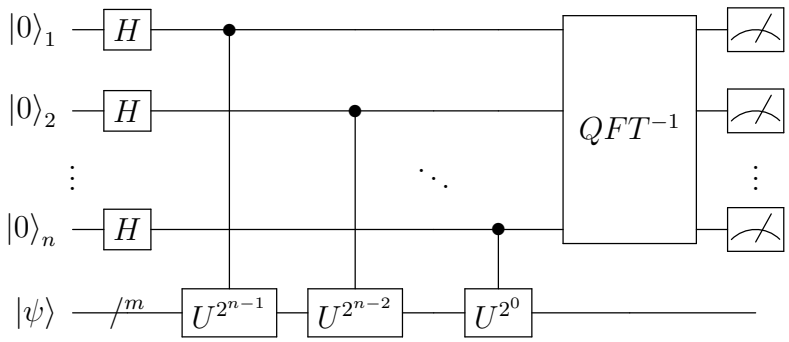

Figure 1: *Circuit for the QPE algorithm [13].*

The symbol $/^m$ denotes that the bottom line corresponds to a subsystem of m qubits. The controlled U^{2^k} gates correspond to the operator $\hat{U}^{2^k}$ on that m qubit subsystem, controlled by one of the top n "ancilla" qubits.

The QFT^{-1} gate corresponds to an inverse quantum Fourier transform on the ancilla qubits. Writing a generic n-qubit state $|\phi\rangle$ as a superposition over all measurement basis states $\{|0\rangle, |1\rangle, |N-1\rangle\}$, where $N = 2^n$ and we are using a shorthand notation for the basis states,

$$\left|\sum_{k=0}^{n-1} 2^k x_k\right\rangle \coloneqq |x_0\rangle \otimes |x_1\rangle \otimes \ldots \otimes |x_{n-1}\rangle\,,\ x_k \in \{0,1\}\,, \tag{1}$$

the inverse quantum Fourier transform is defined by [9]

$$QFT^{-1}\,|\phi\rangle = QFT^{-1} \sum_{j=0}^{N-1} c_j\,|j\rangle \coloneqq \frac{1}{\sqrt{N}} \sum_{j=0}^{N-1}\sum_{k=0}^{N-1} c_j e^{-\frac{2\pi i j k}{N}}\,|k\rangle\,. \tag{2}$$

The final measurement on the ancillas can be shown to yield the correct value of $2^n\theta$ to a precision of $\mathcal{O}(1/N)$, where $\hat{U}\,|\psi\rangle = e^{2\pi i\theta}\,|\psi\rangle$, with a probability of at least $4/\pi^2 \approx 0.405$ [9].

It is possible to reshape the n-ancilla QPE circuit into an iterative, single-ancilla alternative. The existence of the QFT^{-1} gate means the measurements of the ancillas aren't independent, and so an extra classically controlled phase correction is required on each iteration. We shall see that the rodeo algorithm does not require such an addition when transformed into its iterative counterpart.

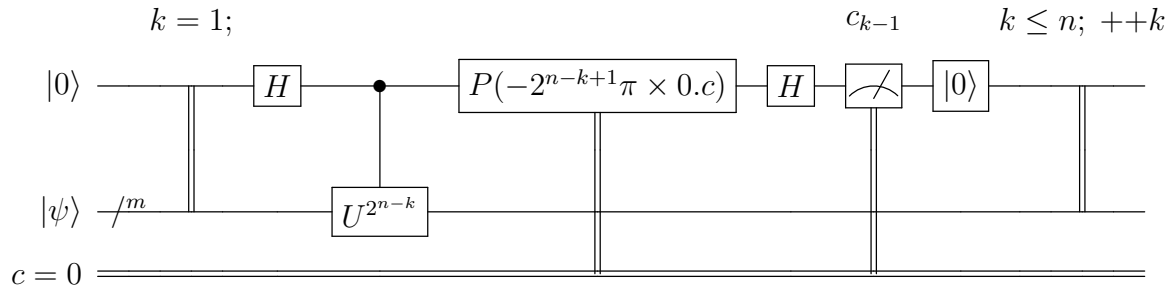

Figure 2: *Iterative circuit for the QPE algorithm. The instructions between the vertical bars at the start and end of the diagram are repeated for values of k from 1 to n, inclusive. The classical register c is initialised to 0, and can be represented by the bit string $c_{n-1}c_{n-2}\ldots c_0$. The k^{th} measurement result is saved to the c_{k-1} bit, and the expression $0.c$ in the classically controlled phase gate's argument is the base-2 decimal $0.c_{n-1}c_{n-2}\ldots c_0$.*

The original QPE algorithm has been modified in various ways, making use of Bayesian inference or other classical post-processing techniques, to achieve improvements such as reducing the number of iterations of the single-ancilla circuit required to measure the phase with a particular precision, or increasing the resistance to gate noise [18] [16].

Although effective for determining the eigenvalues of a unitary operator, neither the original algorithm nor the modifications of the form mentioned above are able to efficiently prepare an eigenstate of the operator $\hat{U}$ associated with a known eigenvalue. An example of the difficulty faced can be found in the paper by Zhao et al. detailing a QPE-based state preparation algorithm, which uses a number of elementary gates exponential in the number of qubits [19].

3 The Rodeo Algorithm

The rodeo algorithm, introduced in 2020 by Choi et al. [4], manages to potentially solve the issue. It replaces the original controlled-U evolution stage with a stochastic evolution using random variables t_k as parameters, and no longer requires the inverse quantum Fourier transform on the ancilla register, instead just using Hadamard gates. The circuit diagram is shown in figure 3. It should be noted that the circuit proposed in the original rodeo paper uses an initial ancilla register state of $|11\ldots1\rangle$ rather than $|00\ldots0\rangle$, but the follow-up paper, in which the algorithm is implemented on IBM Q hardware, switches to using the latter to reduce the impact of noise; the changes made to the classical post-processing are trivial [11].

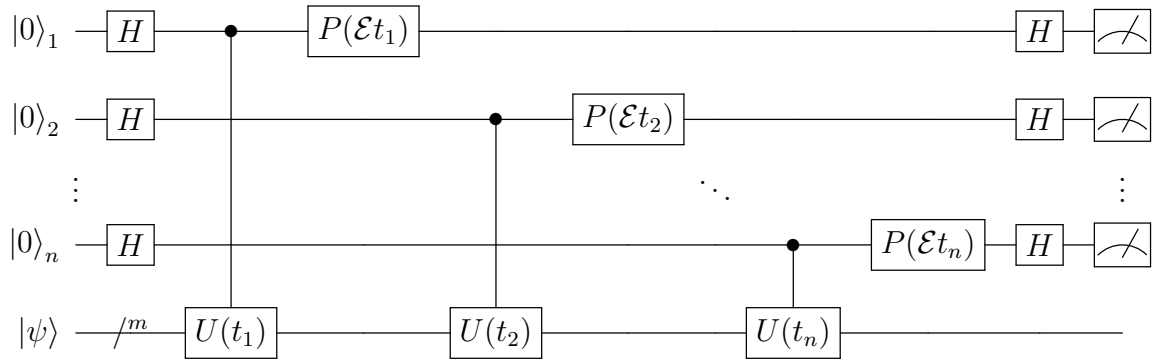

Figure 3: *Circuit for the rodeo algorithm.*

The H and $P(\mathcal{E}t_k)$ gates are Hadamard and phase shift gates, respectively, the actions of which on a one-qubit subsystem are

$$\hat{H}:\ \alpha|0\rangle+\beta|1\rangle\rightarrow\frac{1}{\sqrt{2}}\left[(\alpha+\beta)|0\rangle+(\alpha-\beta)|1\rangle\right], \tag{3}$$

$$\hat{P}(\mathcal{E}t_k):\ \alpha|0\rangle+\beta|1\rangle\rightarrow\alpha|0\rangle+\beta e^{i\mathcal{E}t_k}|1\rangle. \tag{4}$$

The energy $\mathcal{E}$ is called the "target energy", for reasons which will become clear. Finally, the unitary operator $\hat{U}(t_k)$ takes the form

$$\hat{U}(t_k)\coloneqq e^{-i\hat{\mathcal{H}}t_k}. \tag{5}$$

This means that $\hat{U}(t_k)$ corresponds to the evolution of the bottom, "object" register of m qubits under the Hamiltonian $\hat{\mathcal{H}}$ for a time t_k. This algorithm is designed to determine the eigenvalues E_j and prepare the eigenstates $|E_j\rangle$ of this Hamiltonian.

3.1 A Rodeo Cycle

We now analyse the actions of the gates in the circuit. The initial state of the ancillas is $|0\rangle^{\otimes n}$ and the initial object state is $|\psi\rangle$. First, each of the ancillas are acted on by a Hadamard gate:

$$\hat{H}^{\otimes n} \otimes \hat{\mathbb{1}}^{\otimes m} : \ |0\rangle^{\otimes n} \otimes |\psi\rangle \rightarrow |+\rangle^{\otimes n} \otimes |\psi\rangle \,, \tag{6}$$

Where $|+\rangle \coloneqq (|0\rangle + |1\rangle)/\sqrt{2}$. Next, the object state undergoes a series of time evolutions controlled by each of the ancillas. Representing $|\psi\rangle$ as a sum over the eigenstates $|E_j\rangle$ of the Hamiltonian, we have

$$\hat{CU}(t_k) \coloneqq \left(\hat{\mathbb{1}}^{\otimes(k-1)} \otimes |0\rangle\langle 0| \otimes \hat{\mathbb{1}}^{\otimes(n-k)}\right) \otimes \hat{\mathbb{1}}^{\otimes m} + \left(\hat{\mathbb{1}}^{\otimes(k-1)} \otimes |1\rangle\langle 1| \otimes \hat{\mathbb{1}}^{\otimes(n-k)}\right) \otimes e^{-i\hat{\mathcal{H}}t_k}, \tag{7}$$

$$\prod_{k=1}^{n} \hat{CU}(t_k) : \ |+\rangle^{\otimes n} \otimes \sum_j \alpha_j |E_j\rangle \rightarrow \sum_j \alpha_j \left[\bigotimes_{k=1}^{n} \frac{1}{\sqrt{2}} \left(|0\rangle + e^{-iE_j t_k} |1\rangle\right)\right] \otimes |E_j\rangle \,. \tag{8}$$

We then have a phase gate act on each of the ancillas:

$$\left[\bigotimes_{k=1}^{n} \hat{P}(\mathcal{E}t_k)\right] \otimes \hat{\mathbb{1}}^{\otimes m} : \ \sum_j \alpha_j [\ldots] \otimes |E_j\rangle \rightarrow \sum_j \alpha_j \left[\bigotimes_{k=1}^{n} \frac{1}{\sqrt{2}} \left(|0\rangle + e^{i(\mathcal{E}-E_j)t_k} |1\rangle\right)\right] \otimes |E_j\rangle \,. \tag{9}$$

Finally, another Hadamard acts on each of the ancillas:

$$\hat{H}^{\otimes n} \otimes \hat{\mathbb{1}}^{\otimes m} : \ \sum_j \alpha_j [\ldots] \otimes |E_j\rangle \rightarrow |\Psi'\rangle \,, \tag{10}$$

$$|\Psi'\rangle \coloneqq \sum_j \alpha_j \left[\bigotimes_{k=1}^{n} \left|A^j_{(k)}\right\rangle\right] \otimes |E_j\rangle \,, \tag{11}$$

$$\left|A^j_{(k)}\right\rangle \coloneqq \frac{1 + e^{i(\mathcal{E}-E_j)t_k}}{2} |0\rangle + \frac{1 - e^{i(\mathcal{E}-E_j)t_k}}{2} |1\rangle \,. \tag{12}$$

We can now calculate the independent probability of measuring all of the ancillas in the $|0\rangle$ state. We first find the reduced density matrix for the ancillas:

$$\hat{\rho}_{anc;obj} = |\Psi'\rangle \langle \Psi'| \,, \tag{13}$$

$$\hat{\rho}_{anc;obj} = \sum_j |\alpha_j|^2 \left[\bigotimes_{k=1}^{n} \left| A^j_{(k)} \right\rangle \left\langle A^j_{(k)} \right| \right] \otimes |E_j\rangle \langle E_j| \; + \; crossterms, \tag{14}$$

$$\hat{\rho}_{anc} = \mathrm{Tr}_{obj} \left\{ \hat{\rho}_{anc;obj} \right\}, \tag{15}$$

$$\hat{\rho}_{anc} = \sum_j |\alpha_j|^2 \bigotimes_{k=1}^{n} \left| A^j_{(k)} \right\rangle \left\langle A^j_{(k)} \right|, \tag{16}$$

$$\hat{\rho}_{anc} = \sum_j |\alpha_j|^2 \left[\bigotimes_{k=1}^{n} \left(\cos^2 \left[\frac{(\mathcal{E} - E_j)\, t_k}{2} \right] |0\rangle \langle 0| \right) \; + \; \ldots \right]. \tag{17}$$

We now read off that the probability of measuring all ancillas in the $|0\rangle$ state is

$$P_n = \sum_j |\alpha_j|^2 \prod_{k=1}^{n} \cos^2 \left[\frac{(\mathcal{E} - E_j)\, t_k}{2} \right]. \tag{18}$$

Since the final state of the ancillas is separable, we can trivially replace our n-ancilla rodeo circuit with a single-ancilla iterative version. After measuring the ancilla, we reset its state to $|0\rangle$ and repeat the circuit. Iterating this procedure n times will evolve the object register in the same way as if we had used the original n-ancilla circuit. Each iteration of this alternative circuit is referred to as a "rodeo cycle".

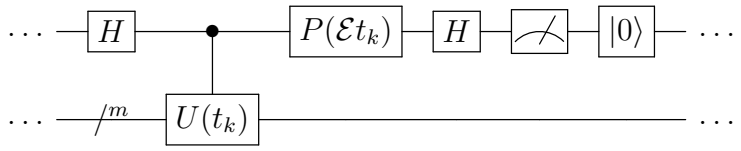

Figure 4: *Circuit for a cycle of the iterative rodeo algorithm.*

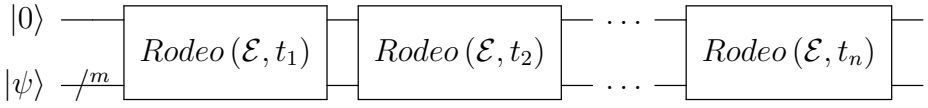

Figure 5: *Circuit for the n-repeat iterative rodeo algorithm. Each Rodeo $(\mathcal{E}, t_k)$ block corresponds to a rodeo cycle.*

3.2 Energy Eigenvalue Filtering

We now analyse the statistics of P_n. For a particular evolution time t_k, choices of the target energy $\mathcal{E}$ which satisfy $(\mathcal{E} - E_j)\, t_k = 2\pi q$, where E_j is a particular energy eigenvalue and $q \in \mathbb{Z}$, will have the maximum contribution from the j^{th} eigenstate to the probability of measuring zero at the end of a rodeo cycle. Since the evolution times $\{t_1, t_2, \ldots, t_n\}$ will be randomly selected, only the choice $\mathcal{E} = E_j$ (that is, $q = 0$) will have the maximum j^{th} contribution to the probability of measuring all zeroes. An example of this for the case that the initial object state $|\psi\rangle$ is an energy eigenstate is illustrated in figure 2 of the original rodeo paper [4].

For choices of $\mathcal{E}$ away from any E_j, the probability of measuring all zeroes depends on the way in which the random evolution times are chosen, the number of rodeo cycles and the number of energy eigenstates contributing to the initial object state. The sampling of a normal distribution is used to generate the evolution times in the original rodeo paper; later, we will explore why this choice is a good one.

The expression for P_n when the initial object state is a sum over s energy eigenstates, with equal amplitudes for simplicity, is

$$P_n = \frac{1}{s} \sum_{j=1}^{s} \prod_{k=1}^{n} \cos^2 \left[\frac{(\mathcal{E} - E_j)\, t_k}{2} \right]. \tag{19}$$

If we assume the cosine arguments $(\mathcal{E} - E_j)\, t_k/2$ modulo 2π are approximately uniform on the interval $[0, 2\pi]$, then P_n becomes the mean of s products of n random samples of $\cos^2(\theta)$.

As explained in the original rodeo paper, For large n, the n^{th} root of P_n is approximated by the geometric mean of $\cos^2(\theta)$ [4],

$$\lim_{n\to\infty} \sqrt[n]{\cos^2(\theta_1) \cos^2(\theta_2) \ldots \cos^2(\theta_n)} \to \exp\left(\frac{1}{2\pi} \int_0^{2\pi} \ln \cos^2(\theta)\, d\theta \right) = \frac{1}{4}, \tag{20}$$

so P_n itself can be approximated by 4^{-n}. For large s, the n^{th} root of P_n is instead approximated by the arithmetic mean of $\cos^2(\theta)$,

$$\lim_{s\to\infty} \frac{\cos^2(\theta_1) + \cos^2(\theta_2) + \ldots + \cos^2(\theta_s)}{s} \to \frac{1}{2\pi} \int_0^{2\pi} \cos^2(\theta)\, d\theta = \frac{1}{2}, \tag{21}$$

allowing P_n to be approximated by 2^{-n}. Figures 6 and 7 show how the accuracy of these two expressions depends on n and s. Regardless of which is more accurate for a particular initial state and number of rodeo cycles, the suppression of the probability of measuring all zeroes away from eigenvalues is exponential in the number of ancillas.

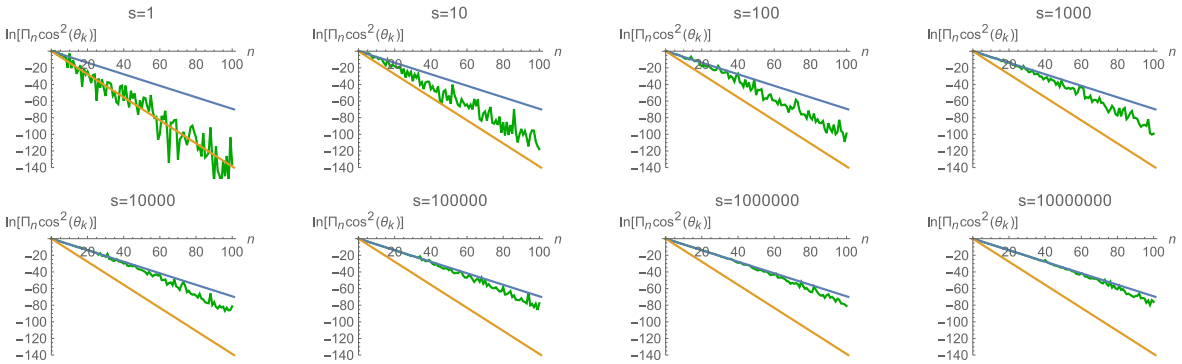

Figure 6: *Plots of the logarithm of sample means of* $\prod_n \cos^2(\theta_k)$ *up to* $n = 100$ *for different sample sizes* s*. The blue and orange lines have gradients* $-\ln 2$ *and* $-\ln 4$*, respectively.*

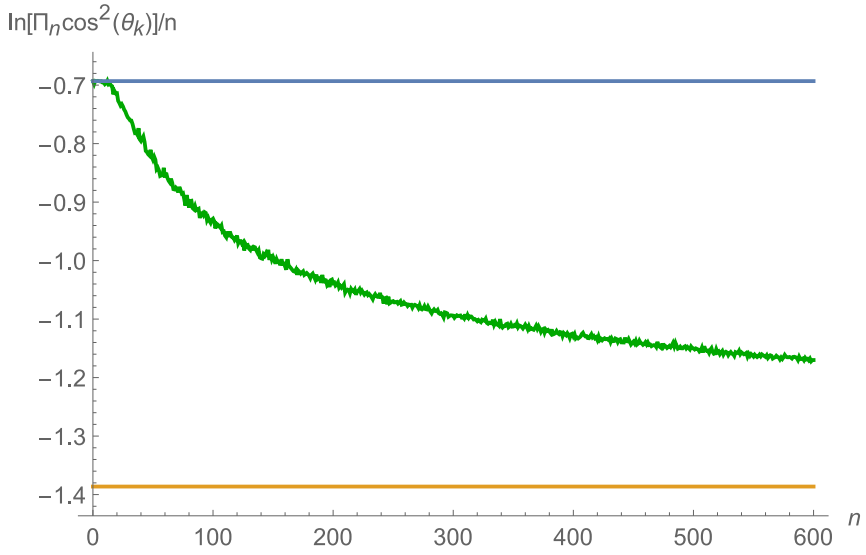

Figure 7: *Plot of the logarithm of the* n^{th} *root of the mean of an* n*-size sample of* $\prod_n \cos^2(\theta_k)$*, showing how the base of the exponential tends away from* 2 *and towards* 4 *if* s *is equal to* n*. The blue and orange lines denote* $-\ln 2$ *and* $-\ln 4$*, respectively.*

Returning briefly to the assumption of the distribution of the cosine arguments modulo 2π being approximately uniform, we can calculate the arithmetic and geometric means of $\cos^2(\theta)$ for different choices of standard deviation for the normal distribution from which the angles are generated, and find the choice at which the distribution achieves what the original rodeo paper refers to as "asymptotic scaling".

While the arithmetic mean can be calculated analytically to be

$$\int_{-\infty}^{\infty} \cos^2(\theta)\, f_{\mathcal{N}_\sigma}(\theta)\, d\theta = \frac{1}{2}\left(1 + e^{-2\sigma^2}\right), \tag{22}$$

where $f_{\mathcal{N}_\sigma}$ is the PDF of a normal distribution with a mean of zero and a standard deviation of σ, the geometric mean can not be expressed in terms of standard functions, but can still be calculated numerically (this is the case for any integral). Both are plotted in figure 8. We find that for standard deviations larger than about 1.5, asymptotic scaling is achieved. This explains the characteristics of the plotted lines in figure 3 of the original rodeo paper.

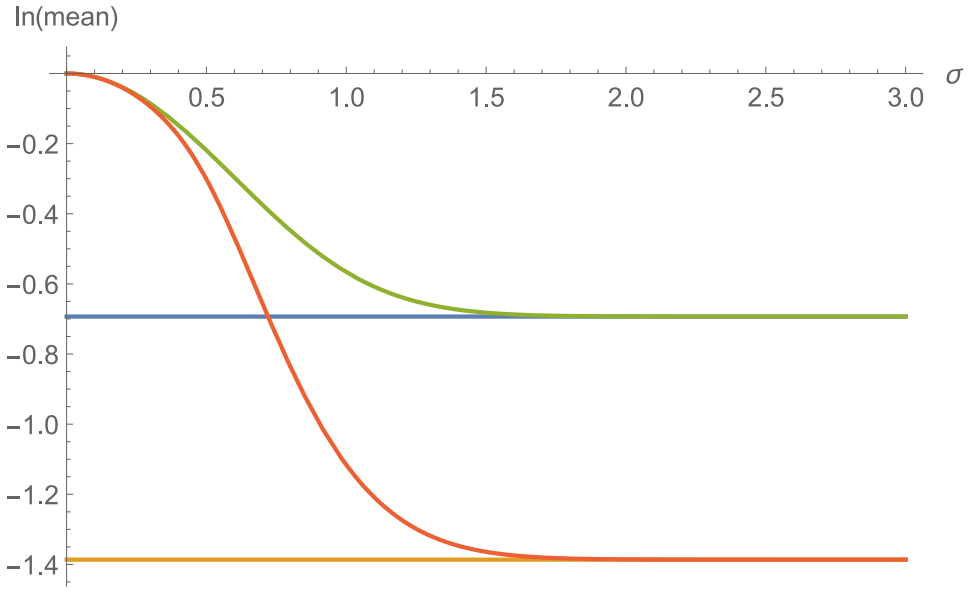

Figure 8: *Plots of the logarithm of the arithmetic and geometric means of* $\cos^2(\theta)$ *in green and red, respectively. The blue and orange lines denote* $-\ln 2$ *and* $-\ln 4$*, respectively.*

3.3 Sequential Rodeo Scanning

The full rodeo algorithm consists of running the circuit with sequences of different parameters to find energy eigenvalues with a desired precision, and to then prepare the associated energy eigenstates. The initial object state is assumed to be prepared at the beginning of each circuit run; initial states with reasonable overlaps with particular targeted eigenstates may be determined from physical considerations of the Hamiltonian, and potentially augmented by other subroutines such as a variational quantum eigensolver (VQE) [10].

The algorithm consists of a series of "rodeo scans". The circuit is ran over a discretised interval of target energies $\mathcal{E}$, with some initial choice of standard deviation σ for the n randomly generated evolution times for each rodeo cycle; again assuming the use of a normal distribution $\mathcal{N}_\sigma$, we find the expectation value of the contribution of the j^{th} eigenstate to the probability of measuring zero for a particular rodeo cycle to be approximately proportional to

$$\int_{-\infty}^{\infty} \cos^2\left[\frac{(\mathcal{E}-E_j)\,t}{2}\right] f_{\mathcal{N}_\sigma}(t)\,dt = \frac{1}{2}\left(1+e^{-\frac{1}{2}\sigma^2(\mathcal{E}-E_j)^2}\right). \tag{23}$$

Since the width of a Gaussian is its standard deviation, and the width when raised to the n^{th} power is reduced by a factor of $\sqrt{n}$, the widths of the peaks in P_n at energy eigenvalues will be approximately equal to $1/(\sigma\sqrt{n})$. Therefore, the discretisation of the target energy interval to initially scan should be comprised of bins of width no less than this. For each bin, a chosen number of "evaluation repeats" are performed, each using a random array of evolution times and consisting of a chosen number of repeated circuit runs, often referred to as the number of "shots".

Once the initial scan has revealed the approximate positions of the eigenvalues, we can reduce the size of the interval of scanned energies by a "narrowing factor", and carry out another scan centred on the desired eigenvalue with the same number of bins, and thus use a standard deviation for the evolution times increased by the same narrowing factor. With each scan, the target energy interval becomes exponentially focused on the eigenvalue.

It is possible that the initial scan does not have the resolution to distinguish nearby eigenvalues. In such a scenario, focusing on the associated peak enough times will allow them to be resolved. An example is shown in figure 9.

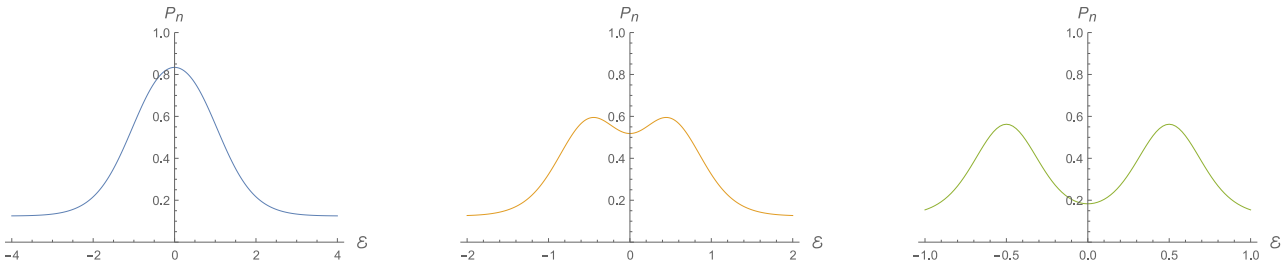

Figure 9: *Plots demonstrating an example of the resolution of two equal-amplitude peaks after a sequence of scans, with* $n = 3$*. The two energy eigenvalues are at* $-1/2$ *and* $1/2$*, the initial choice of* σ *is* 1*, and the narrowing factor is* 2*.*

For large n, there are at least three contributions to the computational complexity for carrying out iterations until reaching a scanning interval of $[E_j - \varepsilon, E_j + \varepsilon]$, or equivalently, determining the the eigenvalue E_j to within an error of ε. First, the total number of scans scales as $\mathcal{O}(\ln \varepsilon)$ due to the multiplicative narrowing factor. Second, the total time evolution over all scans scales as $\mathcal{O}(1/\varepsilon)$ due to the exponential increase in the standard deviation of evolution times with each scan. Third, if the eigenstate has overlap p with the initial object state, the ratio of the height of the peak to the background noise will be approximately

$$\frac{p + 4^{-n}(1-p)}{4^{-n}} = (4^n - 1)p + 1. \tag{24}$$

This tends towards being proportional to p for large n, and so distinguishing the peak from the background noise introduces a factor $\mathcal{O}(1/p)$. The original rodeo paper suggests that there is an additional factor of $\mathcal{O}(\ln \varepsilon)$, but the origin of this term is unclear (this additional factor could instead be $\mathcal{O}\left(\ln^2 \varepsilon\right)$ depending on the interpretation of the argument starting at the end of page 2, but it seems reasonable to assume this is due to an elementary mistake in the writing) [4]. Therefore, we can say that the time complexity of measuring an energy eigenvalue, corresponding to an eigenstate with initial overlap p, within an error of ε is at most

$$\mathcal{O}\left(\frac{\ln^2 \varepsilon}{p\varepsilon}\right). \tag{25}$$

This in itself is not an improvement over conventional QPE. However, we do have a quantum state preparation scheme with a time complexity that is exponentially faster in the magnitude of the desired residual orthogonal amplitude, labelled Δ, than the algorithms based on conventional phase estimation discussed in section 2. After performing enough rodeo scans so that the target eigenstate's energy is know to within an error smaller than the next-nearest energy eigenvalue, we can perform rodeo cycles on this small interval, using

a standard deviation for the evolution times proportional to $1/\varepsilon$, to amplify the amplitude for the target eigenstate.

The first contribution to the time complexity of the state preparation is $\mathcal{O}(1/p)$, as the probability of successfully measuring all zeroes and preparing the eigenstate is proportional to the initial overlap. To calculate the dependence on Δ, we return to the expression for the final state $|\Psi'\rangle$ of the combined system in equation (11) to calculate the overlap with the target eigenstate when zero is measured for all rodeo cycles. We first project out the parts of the ancilla states corresponding to measuring any ones and normalising with $\hat{\mathcal{N}}$:

$$\hat{\mathcal{P}}_{A\to 0} \coloneqq (|0\rangle\langle 0|)^{\otimes n} \otimes \hat{\mathbb{1}}^{\otimes m}, \tag{26}$$

$$\hat{\mathcal{N}}\left\{\hat{\mathcal{P}}_{A\to 0}|\Psi'\rangle\right\} \coloneqq |0\rangle^{\otimes n} \otimes |\psi'_{0^n}\rangle = \frac{1}{P_n}\sum_j \alpha_j \left[\bigotimes_{k=1}^{n} \frac{1+e^{i(\mathcal{E}-E_j)t_k}}{2}|0\rangle\right] \otimes |E_j\rangle\,. \tag{27}$$

The overlap with the j^{th} eigenstate is then

$$|\langle E_j|\psi'_{0^n}\rangle|^2 = \frac{|\alpha_j|^2 \prod_{k=1}^{n} \cos^2\left[\frac{(\mathcal{E}-E_j)t_k}{2}\right]}{\sum_{j'}|\alpha_{j'}|^2 \prod_{k'=1}^{n}\cos^2\left[\frac{(\mathcal{E}-E_{j'})t_{k'}}{2}\right]} \tag{28}$$

Using our assumption that all other energy eigenvalues are outside the scanning interval and the standard deviation for the evolution times is large enough that the contributions from those other eigenstates are exponentially suppressed, this overlap can be well approximated by

$$|\langle E_j|\psi'_{0^n}\rangle|^2 \approx \frac{|\alpha_j|^2}{|\alpha_j|^2 + 4^{-n}\left(1-|\alpha_j|^2\right)}. \tag{29}$$

Labelling $|\alpha_j|^2$ as the initial overlap p, we then recover the original rodeo paper's expression for the estimation of the magnitude of the residual orthogonal amplitude, Δ [4]:

$$\Delta = \sqrt{1-|\langle E_j|\psi'_{0^n}\rangle|^2} \approx F_G \coloneqq \sqrt{\frac{4^{-n}(1-p)}{p+4^{-n}(1-p)}}. \tag{30}$$

The alternative expression, F_A, where the factors of 4^{-n} are replaced with factors of 2^{-n}, is more accurate for the case where the number of rodeo cycles is small or the number of orthogonal eigenstates with non-zero initial amplitudes is very large, as discussed in section 3.2.

The derivative of the logarithm of F_G with respect to n is

$$\frac{d}{dn}\ln F_G = -\frac{4^n p \ln 2}{1 + p\left(4^n - 1\right)}, \tag{31}$$

which approaches a negative constant in the limit of large n. Since the total evolution time is proportional to the number of rodeo cycles, the other contribution to the time complexity is $\mathcal{O}\left(\ln \Delta\right)$, yielding an overall complexity for preparing an eigenstate corresponding to a known eigenvalue, with initial overlap p and a residual orthogonal component with an amplitude of magnitude Δ, of

$$\mathcal{O}\left(\frac{\ln \Delta}{p}\right). \tag{32}$$

This is exponentially faster for $\Delta \to 0$ than both conventional phase estimation and adiabatic methods, which have time complexities of $\mathcal{O}\left(1/\left(p\Delta\right)\right)$ and $\mathcal{O}\left(f\left(p\right)/\Delta\right)$, respectively, where $f\left(p\right)$ is some function of p depending on the details of the adiabatic system [11].

4 Exploring an Example

Given that the properties of the Rodeo algorithm are not particularly sensitive to the size of the object system (apart from the increase in the number of eigenstates with non-zero initial amplitude, which can be combatted by using more rodeo cycles), we can use a basic single-qubit system to explore various details which don't arise from taking limits of large numbers of rodeo cycles or initially overlapping eigenstates. We will assume the use of a large number of evaluation repeats so that the suppression of P_n away from energy eigenvalues is described accurately by using the arithmetic expectation values of squared cosines.

4.1 A Simple System

The Hamiltonian to be used is $\hat{\mathcal{H}} = \omega\hat{\sigma}_x$, where $\hat{\sigma}_x$ is the Pauli X-matrix. The eigenstates and associated eigenvalues are characterised by

$$\hat{\mathcal{H}}\left|\pm\right\rangle = \pm\omega\left|\pm\right\rangle, \tag{33}$$

$$\left|\pm\right\rangle \coloneqq \frac{1}{\sqrt{2}}\left(\left|0\right\rangle \pm \left|1\right\rangle\right). \tag{34}$$

The object state is initialised as

$$|\psi\rangle = \alpha\,|+\rangle + \beta\,|-\rangle\,, \tag{35}$$

which gives us the following expression for the expectation value of measuring all zeroes:

$$\overline{P_n} = \int_{-\infty}^{\infty} \left(|\alpha|^2 \prod_{k=1}^{n} \cos^2\left[\frac{(\mathcal{E}-\omega)\,t_k}{2}\right] + |\beta|^2 \prod_{k'=1}^{n} \cos^2\left[\frac{(\mathcal{E}+\omega)\,t_{k'}}{2}\right] \right) \prod_{k''=1}^{n} f_\sigma\left(t_{k''}\right) dt_{k''}, \tag{36}$$

where f_σ is the PDF of the distribution, with a standard deviation of σ, from which the evolution times are generated. Notice that because $\cos^2(x/2) = (1+\cos x)/2$, this is just a sum of products over the Fourier cosine transforms of the PDF:

$$\overline{P_n} = |\alpha|^2 \left[\frac{1}{2}\left(1 + \mathcal{F}\left\{f_\sigma\right\}\left[\frac{\mathcal{E}-\omega}{2\pi}\right]\right)\right]^n + |\beta|^2 \left[\frac{1}{2}\left(1 + \mathcal{F}\left\{f_\sigma\right\}\left[\frac{\mathcal{E}+\omega}{2\pi}\right]\right)\right]^n, \tag{37}$$

We can also write the expression for the expectation value of the overlap with the $|+\rangle$ eigenstate,

$$\overline{|\langle +|\psi'_{0^n}\rangle|^2} = \int_{-\infty}^{\infty} \left(1 + \frac{|\beta|^2}{|\alpha|^2} \prod_{k=1}^{n} \frac{\cos^2\left[\frac{(\mathcal{E}+\omega)t_k}{2}\right]}{\cos^2\left[\frac{(\mathcal{E}-\omega)t_k}{2}\right]}\right)^{-1} \prod_{k'=1}^{n} f_\sigma\left(t_{k'}\right) dt_{k'}. \tag{38}$$

4.2 Choice of Distribution

We will quickly discuss the choice of the distribution used to generate the evolution times. Until section 4.1, we have used a normal distribution $\mathcal{N}_\sigma$ as in the original rodeo paper. By examining the effect of using other distributions, we can determine whether the choice of a normal distribution is favourable or not. The other distributions we will consider are the uniform and arcsine distributions,

$$\mathcal{U}_\sigma \coloneqq \mathcal{U}\left(-\sqrt{3}\sigma, \sqrt{3}\sigma\right), \tag{39}$$

$$f_{\mathcal{U},\sigma}(t) = \begin{cases} \frac{1}{2\sqrt{3}} & -\sqrt{3}\sigma \le t \le \sqrt{3} \\ 0 & otherwise \end{cases}, \tag{40}$$

$$\mathcal{A}_\sigma := \mathcal{A}\left(-\sqrt{2}\sigma, \sqrt{2}\sigma\right), \tag{41}$$

$$f_{\mathcal{A},\sigma}(t) = \begin{cases} \frac{1}{\pi\sqrt{\left(\sqrt{2}\sigma+t\right)\left(\sqrt{2}\sigma-t\right)}} & -\sqrt{2}\sigma \leq t \leq \sqrt{2} \\ 0 & otherwise \end{cases}, \tag{42}$$

where both $\mathcal{U}_\sigma$ and $\mathcal{A}_\sigma$ have been defined to also have a mean of zero and a standard deviation of σ.

The expressions for $\overline{P_n}$ for each of $\mathcal{N}_\sigma$, $\mathcal{U}_\sigma$ and $\mathcal{A}_\sigma$ are

$$\overline{P_{n,\mathcal{N}}} = |\alpha|^2 \left[\frac{1}{2}\left(1 + e^{-\frac{1}{2}\sigma^2(\mathcal{E}-\omega)^2}\right)\right]^n + |\beta|^2 \left[\frac{1}{2}\left(1 + e^{-\frac{1}{2}\sigma^2(\mathcal{E}+\omega)^2}\right)\right]^n, \tag{43}$$

$$\overline{P_{n,\mathcal{U}}} = |\alpha|^2 \left[\frac{1}{2}\left(1 + \text{sinc}\left[\sqrt{3}\sigma\left(\mathcal{E}-\omega\right)\right]\right)\right]^n + |\beta|^2 \left[\frac{1}{2}\left(1 + \text{sinc}\left[\sqrt{3}\sigma\left(\mathcal{E}+\omega\right)\right]\right)\right]^n, \tag{44}$$

$$\overline{P_{n,\mathcal{A}}} = |\alpha|^2 \left[\frac{1}{2}\left(1 + J_0\left[\sqrt{2}\sigma\left(\mathcal{E}-\omega\right)\right]\right)\right]^n + |\beta|^2 \left[\frac{1}{2}\left(1 + J_0\left[\sqrt{2}\sigma\left(\mathcal{E}+\omega\right)\right]\right)\right]^n, \tag{45}$$

where J_0 is a Bessel function of the first kind. Figure 10 shows how $\overline{P_n}$ varies with $\mathcal{E}$ for each distribution, while figure 11 shows how the noise away from a peak varies with σ. Finally, figure 12 shows how the mean magnitude of the residual orthogonal component at a peak varies with σ.

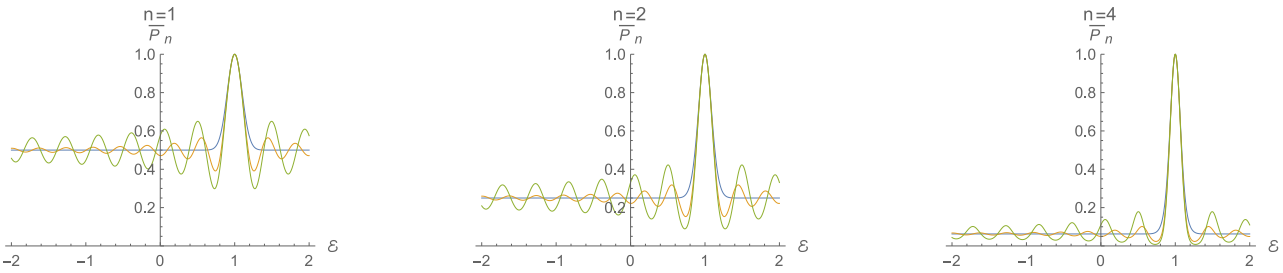

Figure 10: *Plots demonstrating how* $\overline{P_n}$ *varies with* $\mathcal{E}$ *for* $n = 1$, 2 *and* 4. *The plots for the different distributions* $\mathcal{N}_\sigma$, $\mathcal{U}_\sigma$, *and* $\mathcal{A}_\sigma$ *are coloured blue, orange and green, respectively. The fixed parameters are* $\sigma = 10$, $\omega = 1$, $\alpha = 1$, $\beta = 0$.

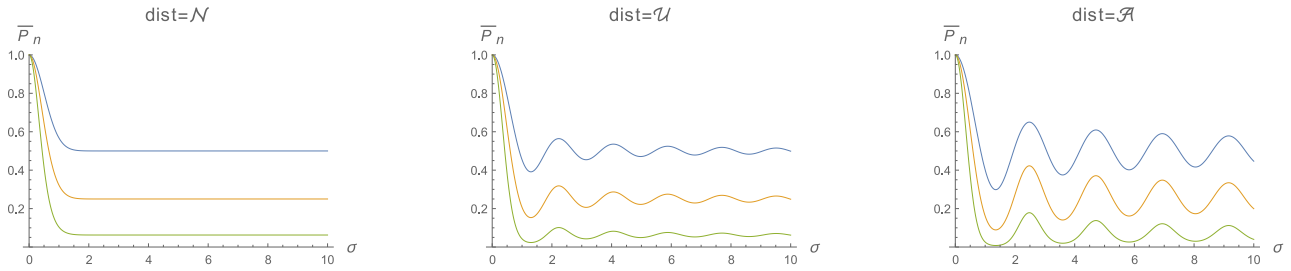

Figure 11: *Plots demonstrating how* $\overline{P_n}$ *varies with* σ *away from an eigenvalue peak for the different distributions* $\mathcal{N}_\sigma$, $\mathcal{U}_\sigma$, *and* $\mathcal{A}_\sigma$. *The plots for* $n = 1$, 2 *and* 4 *are coloured blue, orange and green, respectively. The fixed parameters are* $\mathcal{E} = -1$, $\omega = 1$, $\alpha = 1$, $\beta = 0$.

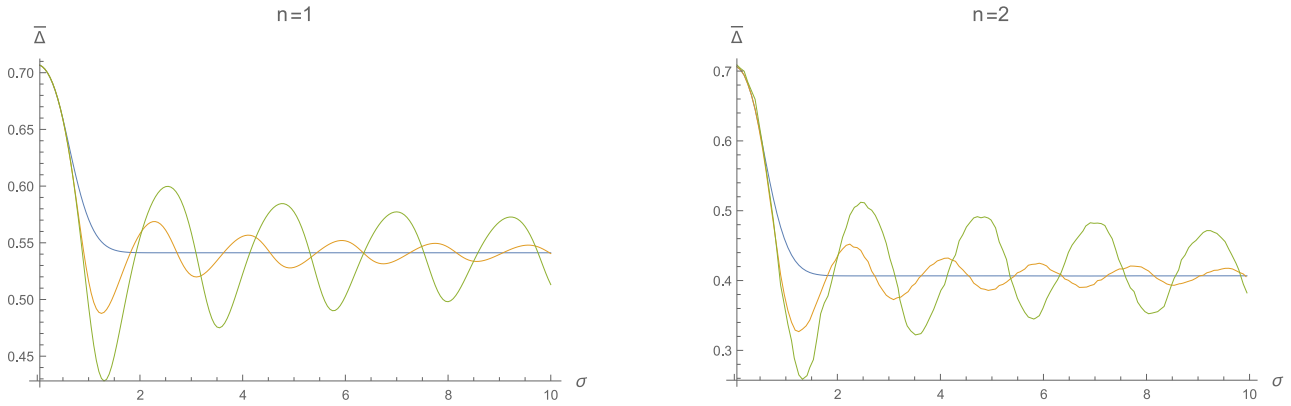

Figure 12: *Plots demonstrating how* $\overline{\Delta}$ *varies with* σ *at an eigenvalue peak for* $n = 1$ *and* 2 *(the numerical integrals required for the* $\mathcal{U}_\sigma$ *and* $\mathcal{A}_\sigma$ *distributions at* $n = 4$ *incurred large noisy errors). The plots for the different distributions* $\mathcal{N}_\sigma$, $\mathcal{U}_\sigma$, *and* $\mathcal{A}_\sigma$ *are coloured blue, orange and green, respectively. The fixed parameters are* $\mathcal{E} = 1$, $\omega = 1$, $\alpha = \beta = 1/\sqrt{2}$.

We can conclude that the choice of a normal distribution is a reasonable one as it avoids the unwanted oscillations in P_n and Δ, that appear when choosing a distribution with an oscillatory Fourier transform. Although the relative magnitudes of these oscillations, and thus the chance of incorrectly identifying the peaks of P_n, decrease as the number of rodeo cycles increases, there is no reason not to choose a distribution which doesn't have these features. An example of another distribution that could be used that has a decaying Fourier transform is the Laplace distribution, but the impact on the performance of the rodeo algorithm as a whole would be barely affected by making such a change.

4.3 Monte Carlo State Preparation Simulation

Stochastic simulations of state preparation for this system demonstrate the exponential speedup granted by the rodeo algorithm. Figure 13 illustrates how effectively the rodeo cycles reduce the overlap with unwanted eigenstates and increase the overlap with the de-

sired one, and figure 14 shows how even very small overlaps with the desired state can be amplified very quickly.

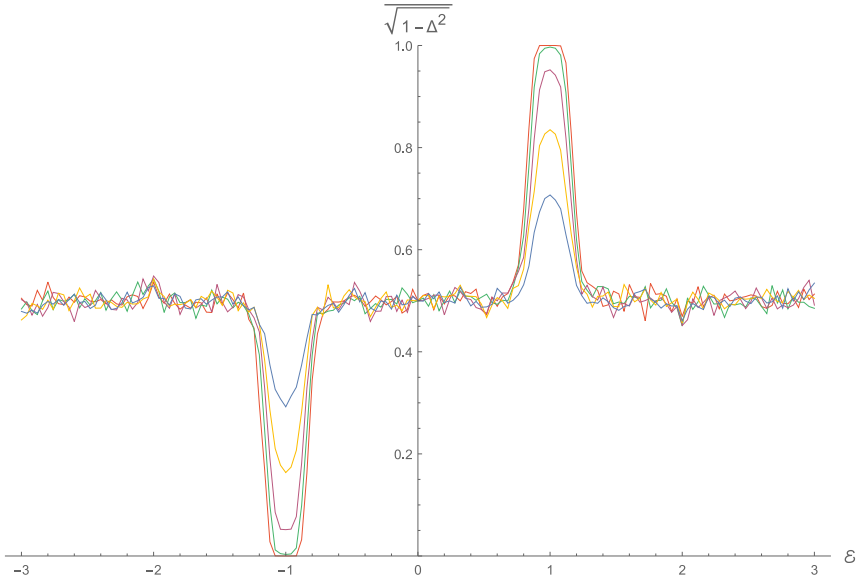

Figure 13: *Plot of the mean of simulated random samples of the overlap with the desired eigenstate* $|+\rangle$ *as a function of target energy* $\mathcal{E}$ *for* 1 *(blue),* 2 *(yellow),* 4 *(purple),* 8 *(green) and* 16 *(red) rodeo cycles.*

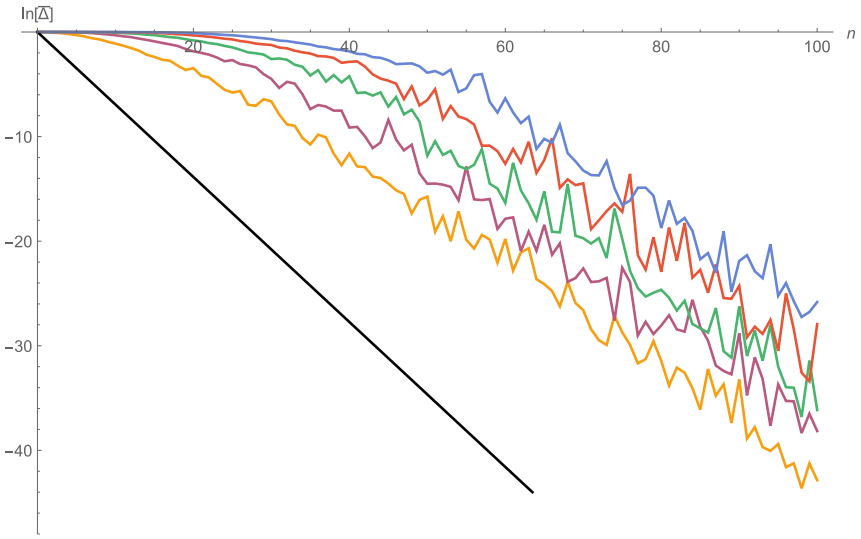

Figure 14: *Plot of the logarithm of the mean of simulated random samples of the magnitude of the residual orthogonal component as a function of the number of rodeo cycles* n *for initial overlaps of* 10^{-3} *(yellow),* 10^{-6} *(purple),* 10^{-9} *(green),* 10^{-12} *(red) and* 10^{-15} *(blue). The black line corresponds to* 2^{-n}*.*

5 IBM Q Device State Preparation

The second rodeo paper from Choi et al. demonstrated the use of the rodeo algorithm for finding the energy eigenstates of a one-qubit Hamiltonian using the IBM Q Casablanca device. We shall attempt to use a simulation of the IBM Q Nairobi device, through `AerSimulator`'s `from_backend` function within Qiskit [12], to find the eigenvalues of a two-qubit Hamiltonian, and then prepare the ground eigenstate. Inspired by the method used to generate the Hamiltonians in the second rodeo paper, we will use a Hamiltonian generated from the random sum of tensor products of Pauli and identity operators. As well as noise arising from gate errors, the circuit will also incur a source of systematic error arising from the Trotterisation of the controlled time evolution [17] [3].

The achieved overlap could be obtained by manipulating the final object states and measuring, but instead we will use a procedure which is a more general method to measure the overlap between two states, namely the "swap test" [1] [2].

The swap test requires another quantum register to hold the energy eigenstate we want to measure the overlap with, and an additional "swap ancilla" on which a measurement is performed. After the Hadamard, controlled swap and other Hadamard gates, the probability of measuring the swap ancilla to be in the state $|0\rangle$, when all rodeo cycles have yielded ancilla measurements of zero, is

$$P_{swap} = \frac{1}{2}\left(1 + |\langle E_j|\psi'_{0^n}\rangle|^2\right). \tag{46}$$

Rearranging to get the magnitude of the residual orthogonal component Δ, we have

$$\Delta = \sqrt{2\,(1 - P_{swap})}. \tag{47}$$

A small caveat with using the swap test is that the target eigenstate $|E_j\rangle$ has to be prepared also, and this process will itself be prone to errors. Employing alternative techniques for measuring the overlap which do not require this explicit state initialisation could be more desirable.

Nevertheless, we first use the sequential rodeo scanning algorithm to find the energy eigenvalues to within a small error. We then amplify the amplitude of the ground state and use the swap test alongside some other classical post-processing to pick out the shots for which all rodeo cycles measured zero, and measure the mean overlap. Ideally a test of this procedure would search a space of Hamiltonians, as is done in the second rodeo paper [11], but no more than one example Hamiltonian could be explored at the current time.

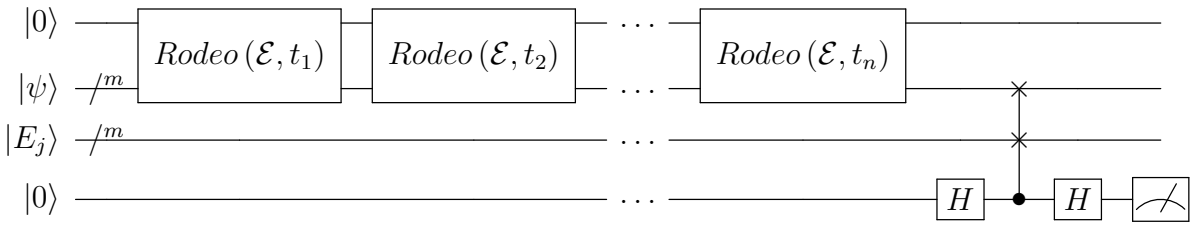

Figure 15: *The iterative rodeo circuit with a swap test appended to assess the accuracy of the state preparation. The bottom ancilla is used to measure the overlap between the final state of the object system and the energy eigenstate* $|E_j\rangle$.

The randomly generated Hamiltonian is equal to

$$\hat{\mathcal{H}} = \tag{48}$$

$$\begin{aligned}
&-0.68388\hat{\mathbb{1}} \otimes \hat{\mathbb{1}} + 0.00054\hat{\mathbb{1}} \otimes \hat{\sigma}_x + 0.63435\hat{\mathbb{1}} \otimes \hat{\sigma}_y + 0.25985\hat{\mathbb{1}} \otimes \hat{\sigma}_z \\
&+0.16555\hat{\sigma}_x \otimes \hat{\mathbb{1}} - 0.72323\hat{\sigma}_x \otimes \hat{\sigma}_x + 0.48794\hat{\sigma}_x \otimes \hat{\sigma}_y + 0.11261\hat{\sigma}_x \otimes \hat{\sigma}_z \\
&+0.06378\hat{\sigma}_y \otimes \hat{\mathbb{1}} - 0.51002\hat{\sigma}_y \otimes \hat{\sigma}_x - 0.78572\hat{\sigma}_y \otimes \hat{\sigma}_y - 0.64711\hat{\sigma}_y \otimes \hat{\sigma}_z \\
&-0.29152\hat{\sigma}_z \otimes \hat{\mathbb{1}} - 0.89286\hat{\sigma}_z \otimes \hat{\sigma}_x - 0.32324\hat{\sigma}_z \otimes \hat{\sigma}_y - 0.95432\hat{\sigma}_z \otimes \hat{\sigma}_z.
\end{aligned}$$

The phase estimation, shown in figure 16, used 8 rodeo cycles, 50 target energy bins, 100 evaluation repeats for each energy bin, and 2048 shots for each evaluation repeat. The positions of the peaks in the P_n measurements are calculated by SciPy's `find_peaks` function [14].

In practice, this phase estimation result would be just one of many rodeo scans focusing in on a yet-unknown energy eigenvalue. However, since we know the eigenvalue, we can skip to testing the state preparation at the lowest-level eigenvalue, with a large choice of the value for σ, at 10000.

We can see in figure 17 that although the suppression of the residual eigenstates is tending towards being logarithmic in the number of rodeo cycles for the non-noisy simulation, the errors in the IBM Q Nairobi simulation runs are large enough that this behaviour is spoiled. Factors that could have caused this is the depth of the circuit becoming too large, and the preparation of the eigenstate for the swap test being inaccurate.

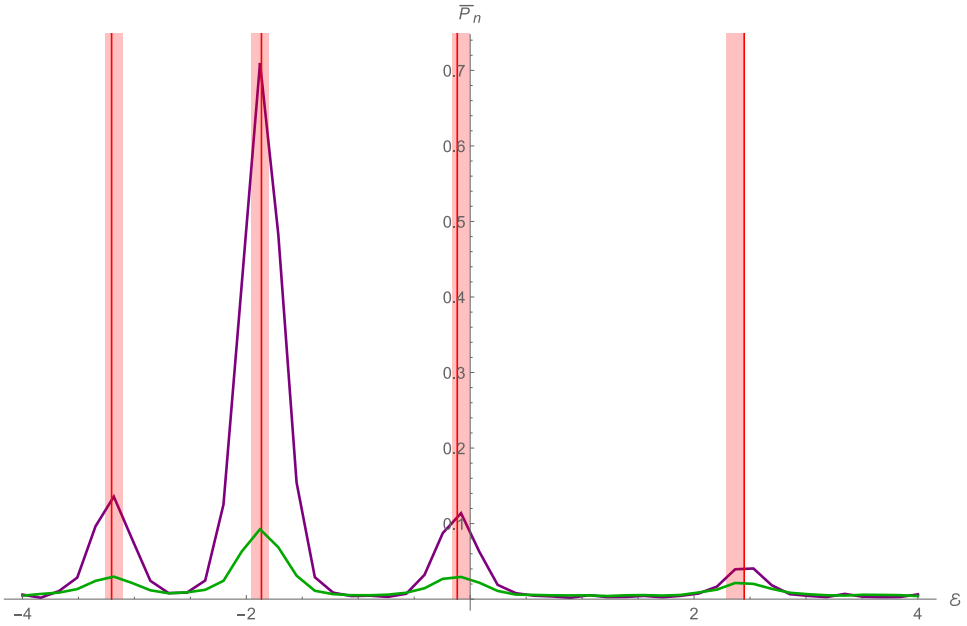

Figure 16: *Plot of the mean probability for measuring all zeros using the simulation of IBM Q Nairobi (green) and a noiseless simulation (purple). The pink columns are centred on the bins that SciPy's peak finding function picked out during the IBM Q Nairobi run, and the red lines are at the energy eigenvalues.*

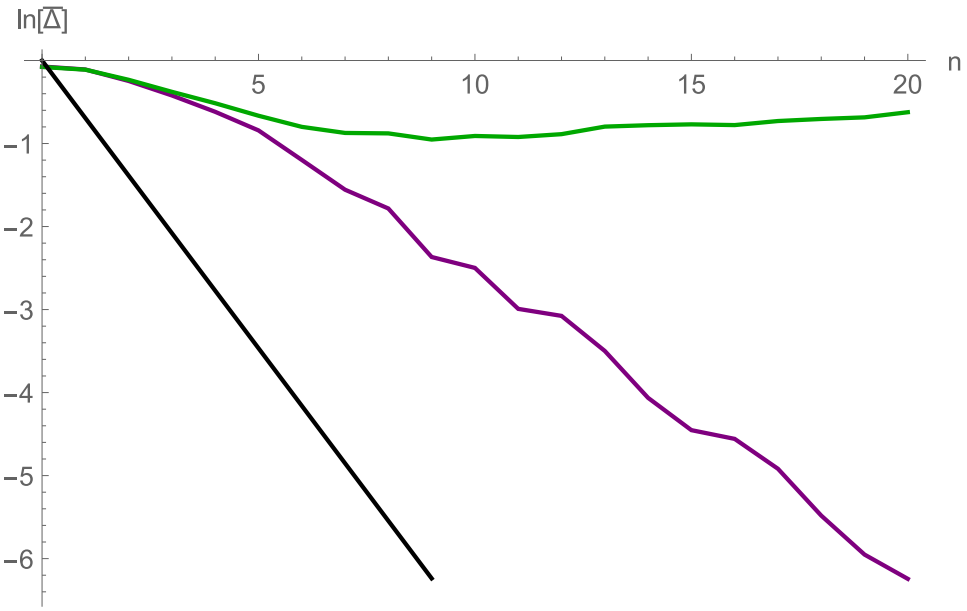

Figure 17: *Plot for the logarithm of the mean magnitude of residual orthogonal component for the simulation of IBM Q Nairobi (green) and a noiseless simulation (purple). The black line corresponds to* 2^{-n}.

6 Conclusion

We have concretised many of the ideas presented in the original two papers on the rodeo algorithm, understanding and explicitly demonstrating the ability for the rodeo algorithm to prepare energy eigenstates in particular. We find that many of the important properties of the algorithm are effectively independent of the number of qubits making up the object state, apart from the expected number of unwanted eigenstates of non-zero initial amplitude while performing phase estimation and the implicit gate complexity of manipulating larger systems. We have also successfully demonstrated quantum phase estimation for a two-qubit system using a simulation of IBM Q hardware, though failed to achieve asymptotically scaling quantum state preparation.

There are plenty more details about the qualities of this algorithm that would be interesting to pursue; in particular, its suitability for preparing eigenstates on less noisy hardware, the ways in which its performance could be improved by additional subroutines before or after the iteration of the rodeo cycles, and the difference in its precision and accuracy between analysing Hamiltonians of different localities.

References

[1] Adriano Barenco, Andre Berthiaume, David Deutsch, Artur, Richard Jozsa, and Chiara Macchiavello. Stabilization of quantum computations by symmetrization, 1997.

[2] Harry Buhrman, Richard Cleve, John Watrous, and Ronald de Wolf. Quantum fingerprinting, 2001.

[3] Andrew M. Childs, Yuan Su, Minh C. Tran, Nathan Wiebe, and Shuchen Zhu. Theory of trotter error with commutator scaling, 2021.

[4] Kenneth Choi, Dean Lee, Joey Bonitati, Zhengrong Qian, and Jacob Watkins. Rodeo algorithm for quantum computing. `https://arxiv.org/abs/2009.04092`, 2020.

[5] Aram W. Harrow, Avinatan Hassidim, and Seth Lloyd. Quantum algorithm for solving linear systems of equations. `https://arxiv.org/abs/quant-ph/9511026`, 2008.

[6] Abhinav Kandala, Antonio Mezzacapo, Kristan Temme, Maika Takita, Markus Brink, Jerry M. Chow, and Jay M. Gambetta. Hardware-efficient variational quantum eigensolver for small molecules and quantum magnets, 2017.

[7] Iordanis Kerenidis and Anupam Prakash. Quantum recommendation systems. https://arxiv.org/abs/1603.08675, 2016.

[8] A. Y. Kitaev. Quantum measurements and the abelian stabilizer problem. https://arxiv.org/abs/quant-ph/9511026, 1995.

[9] Michael A. Nielsen and Isaac L. Chuang. Quantum computation and quantum information: 10th anniversary edition. https://www.cambridge.org/highereducation/books/quantum-computation-and-quantum-information/01E10196D0A682A6AEFFEA52D53BE9AE, 2011.

[10] Alberto Peruzzo, Jarrod McClean, Peter Shadbolt, Man Hong Yung, Xiao Qi Zhou, Peter J. Love, Alán Aspuru-Guzik, and Jeremy L. O'Brien. A variational eigenvalue solver on a photonic quantum processor, 2014.

[11] Zhengrong Qian, Jacob Watkins, Gabriel Given, Joey Bonitati, Kenneth Choi, and Dean Lee. Demonstration of the rodeo algorithm on a quantum computer. https://arxiv.org/abs/2110.07747, 2021.

[12] Qiskit. Aersimulator. https://qiskit.org/documentation/stubs/qiskit.providers.aer.AerSimulator.html.

[13] Qiskit. Quantum phase estimation. https://qiskit.org/textbook/ch-algorithms/quantum-phase-estimation.html.

[14] SciPy. Find peaks. https://docs.scipy.org/doc/scipy/reference/generated/scipy.signal.find_peaks.html.

[15] Peter W. Shor. Algorithms for quantum computation: Discrete logarithms and factoring. https://ieeexplore.ieee.org/document/365700, 1994.

[16] Krysta M. Svore, Matthew B. Hastings, and Michael Freedman. Faster phase estimation, 2014.

[17] H. F. Trotter. On the product of semi-groups of operators, 1959.

[18] Nathan Wiebe and Chris Granade. Efficient bayesian phase estimation. https://journals.aps.org/prl/abstract/10.1103/PhysRevLett.117.010503, 6 2016.

[19] Jian Zhao, Yu-Chun Wu, Guang-Can Guo, and Guo-Ping Guo. State preparation based on quantum phase estimation. https://arxiv.org/abs/1912.05335, 2019.